A remark on the multi-domain hybrid method for calculating the power-law decay of the gravitational radiation waveforms with analytic radiation boundary conditions

Joshua Buli

Department of Mathematics,
State University of New York at Buffalo,
Buffalo, NY 14260-2900, USA
and
Department of Mathematics,
University of California,
Riverside, Riverside, CA 92521, USA
E-mail: jbuli001@ucr.edu

Jae-Hun Jung*

Department of Mathematics,
State University of New York at Buffalo,
Buffalo, NY 14260-2900, USA
E-mail: jaehun@buffalo.edu
*Corresponding author

Debananda Chakraborty

Department of Mathematics,
Virginia Intermont College,
Bristol, Virginia 24201, USA
E-mail: debanandachakraborty@vic.edu

Abstract: A hybrid method based on the multi-domain spectral and finite difference methods is considered for computing the power-law decay of gravitational radiation waveforms. For the radiation boundary condition, we adopt the analytic radiation boundary condition based on the Laplace transformation of kernel functions developed by Lau (2005). In this note, we present several numerical results for the orbital index $l = 2$ with the hybrid and Lau's method. The Lau's method enables the hybrid method to obtain the power-law decay even when the computational domain is small, but the numerical results show that the proper power-law decay rate, $p = 7$ is not obtained. Instead, we obtained $p \sim 4$, which corresponds to the power-law decay rate extracted when the outer domain goes to ∞. We remark that the system of equations or high order method with high precision is necessary for obtaining the proper decay rate.

Copyright 2014 Inderscience Enterprises Ltd.

Keywords: radiation boundary conditions; gravitational radiation waveforms; spectral methods; finite difference methods.

Reference to this paper should be made as follows: Buli, J., Jung, J-H. and Chakraborty, D. (2014) 'A remark on the multi-domain hybrid method for calculating the power-law decay of the gravitational radiation waveforms with analytic radiation boundary conditions', *Int. J. Applied Nonlinear Science*, Vol. 1, No. 2, pp.104–121.

Biographical notes: Joshua Buli received his BS in Mathematics in 2012 from the University at Buffalo, the State University of New York. He is currently a Doctoral student in Mathematics Department at the University of California Riverside.

Jae-Hun Jung is an Assistant Professor of Mathematics at the University at Buffalo, the State University of New York with research areas in numerical analysis and scientific computing.

Debananda Chakraborty is an Assistant Professor of Mathematics at the Virginia Intermont College (VIC). Before joining VIC, he was an Adjunct Instructor of Mathematics at the University at Buffalo. He received his PhD in Applied Mathematics from the University at Buffalo under the supervision of Jae-Hun Jung. His research area is numerical analysis and scientific computing, particularly the spectral methods for PDEs.

1 Introduction

An in-depth understanding of the decay pattern of the gravitational radiation waveforms is important in studying the black-hole system with colliding objects moving toward the black-hole (Baumgarte and Shapiro, 2011). Price showed that the late-time waveform decays according to $t^{-(2l+3)}$, where t is the time and l is the orbital index (Price, 1972). The power of the late-time power-law decay depends on the initial profile of the system (Avalos and Lousto, 2005). The late-time decay pattern is also related to the gravitational theory. For example, the late-time decay of the gravitational wave predicted by the general relativity has a different pattern from the one predicted by the string theory. Thus detecting the late-time decay of the gravitational wave will significantly impact our understanding of the dynamics of the gravitational system and the gravitational theory as well although the experimental complexity is challenging.

Due to the nonlinearity and experimental complexity, it is crucial to construct a reliable computational methodology to calculate the late-time decay of the gravitational radiation. For this, various numerical methods have been developed to calculate accurately the proper decay profile of the gravitational radiation waveforms. For some of the gravitational systems such as the Schwarzschild space-time, the analytic decay patterns are known, which is characterised by the power-law decay following the quasi-normal decay. The developed computational methods are verified by comparing the analytic power-law decays with the computationally obtained late-time decays. The frequency domain approaches, e.g., Glampedakis (2005) yield highly accurate results but the application is only limited to simple cases. Instead, the time-domain approaches

have more flexibility. There are numerous time-domain methods developed. It is not practical to list all of them here but many of them are based on the higher-order finite difference methods including the pioneering works by Davis et al. (1971) and by Lousto and his co-workers (Lousto and Price, 1997).

The main computational difficulty of the time-domain method is to deal with the artificial boundary created by the truncation of the computational domain. For scalar perturbations in the Schwarzschild space-time, the gravitational radiation, $\Psi(\tau)$ propagates according to the second order wave equation in $(1+1)$D coupled with the potential function $V(\rho)$ with the space coordinate ρ and time coordinate τ. The potential function is vanishing as $\rho \to \infty$, but only algebraically. For the time-domain method, the computational domain is truncated at $\rho = \rho_B << \infty$. The boundary condition at ρ_B should satisfy the radiation boundary condition. In $(1+1)$D, the outgoing boundary condition is given by the Sommerfeld boundary condition such as $\Psi_\tau + c\Psi_\rho = 0$ where $c = 1$ when $\rho \to \infty$. However, due to the non-vanishing potential function, the truncation of the computational domain makes the homogeneous Sommerfeld boundary condition insufficient and produces artificial reflections, which prevents the proper power-law decay.

To avoid this problem, one can extend the computational domain large enough so that the potential effect is minimised. However, this approach is costly. In our previous research, we combined the multi-domain spectral method and the finite difference method to reduce the computational cost. We successfully obtained the proper power-law decay with a small value of ρ_B (Chakraborty et al., 2011). The idea of the hybrid method is that the local method, i.e., the finite difference method is used for the boundary domain and the interior domain is taken care of by the global method, e.g., the spectral method. With the hybridisation, we could reduce the boundary effects while maintaining the high-order accuracy. However, this approach may fail when ρ_B is arbitrarily small.

Alternatively, Lau (2004) and Benedict et al. (2012) developed an analytic approach to find the exact radiation boundary condition. Lau used the Laplace transformation of kernel functions and derived the exact radiation boundary conditions. The boundary condition is given in the form of the modified radiation boundary condition in $(1+1)$D by adding the convolution term C in the homogeneous Sommerfeld condition, i.e., $\Psi_\tau + c\Psi_\rho = C(\rho, \tau)$. The convolution function is a function of ρ_B and τ. The convolution function contains the whole history of $\Psi(\tau)$ from $\tau = 0$ at $\rho = \rho_B$. The main advantage of Lau's method is that ρ_B can be arbitrarily small.

In this paper, we adopt Lau's analytic boundary condition in our hybrid method. The main goal of this paper is to apply Lau's analytic boundary condition to our hybrid method in order to further reduce the computational cost by having smaller ρ_B. Combining Lau's boundary condition, we check how our spectral and finite difference hybrid method performs for the small value of ρ_B. We also use the spectral filtering method. For the hybrid method, the exit boundary domain is treated by the finite difference method. The interior domain is treated by the multi-domain spectral method. For the stable patching, we use the fourth order patching conditions. The patching of two adjacent spectral domains is straightforward. For the patching of the spectral and finite difference domains, we use the fourth order finite difference patching using the Lagrange interpolation to address the grid non-uniformity across the finite difference and spectral domain interface. Lau's analytic boundary condition is adopted in the hybrid method by updating the solution at the boundary of the exit domain. The solution at the boundary is obtained from the boundary condition that is given by the first order

wave equation with the convolution term $C(\tau)$ as a source term. The advection part in the left hand side is approximated using the first order finite difference method. The convolution function $C(\tau)$ contains the information of the history of Ψ at ρ_B which is given in an integral form. Instead of saving all the history of the solution at ρ_B to calculate the integral, we use the recursive relation of $C(\tau + \delta\tau) = C(\tau) + \delta C$. For this, Ψ is interpolated using the first order approximation in the interval of $[\tau, \tau + \delta\tau]$, which is more efficient than the direct integration.

For the numerical experiments, we choose the orbital index $l = 2$ and use the Zerilli potential, for which the proper power-law decay has the power of $p = -7$. The computational domain is truncated at $\rho_B = 15$. Note that the value of $\rho_B = 15$ is very small compared to the value of $\rho_B = 387.5$ used in our previous research for the hybrid method (Chakraborty et al., 2011). Our numerical results show that if the first-order Sommerfeld radiation boundary condition is used without Lau's method, no power-law decay was obtained at all. However, when combined with Lau's analytic boundary condition, the hybrid method yields the power decay of $p \sim -4$. But the decay is much slower than the correct decay of $p = -7$. That is, Lau's method makes the hybrid method yield the power-law decay successfully but the correct power was not achieved. We tried several different numerical simulations with various grid resolutions and various values of ρ_B, each of which shows the same result. Thus we remark, in this paper, that our numerical results may imply that high precision is required or more consistent way of numerical method, such as rewriting the given equation into system is required for obtaining the proper power-law decay. The current approach uses the second order wave equation combined with the first order radiation boundary condition. The inconsistency in order in these equations causes significant computational errors at the boundary as shown in the paper. Similar result was reported in Khanna (2013) where increasing the resolution does not yield the proper decay rate. In Khanna (2013), it is shown that the higher precision computation or higher-order formulation are required for obtaining the proper decay order rather than increasing the grid resolution.

This note is organised as follows. In Section 2, we briefly explain Lau's analytic boundary condition. In Section 3, the first order approximation is used to derive the recursion formula for the convolution function. In Section 4, we explain the computational methods adopted in this paper, i.e., the multi-domain spectral and finite difference hybrid method and the spectral filtering method. In Section 5, numerical results are presented. In Section 6, a brief concluding remark is given.

2 Analytic radiation boundary condition: Lau's method

In this work, we will consider the Schwarzschild system. The gravitational wave, Ψ, of the scalar perturbation on the Schwarzschild space-time is a function of dimensionless time and radial distance, denoted by τ and ρ, respectively. These non-dimensional parameters are derived from the physical coordinates of the Schwarzschild space-time with time, t, and radial distance, r, by the following relations

$$t = 2M\tau, \tag{1}$$

$$r = 2M\rho, \tag{2}$$

where $M(=1)$ is the black-hole mass, and we normalise the equation such that the new dimensionless variables defined above, allow the Schwarzschild metric to be re-written as

$$ds^2 = -Fd\tau + F^{-1}d\rho^2 + \rho^2(d\theta^2 + \sin^2\theta d\phi^2), \tag{3}$$

where $F = 1 - \rho^{-1}$, and θ,ϕ are the angular coordinates, which are ignored due to the radial symmetry in this paper. Using the Regge-Wheeler tortoise coordinate, ρ_*, a change in variables can be made using the substitution $\rho_* = \rho - \log(\rho - 1)$. The gravitational wave perturbations abide by the following wave equation with $V^Z(\rho)$ being the Zerilli potential

$$\frac{\partial^2\Psi}{\partial\tau^2} - \frac{\partial^2\Psi}{\partial\rho_*^2} + V^Z(\rho)\Psi = 0. \tag{4}$$

The Zerilli potential, $V^Z(\rho)$ in equation (4) can be exactly described as

$$V^Z(\rho) = \left(1 - \frac{1}{\rho}\right)\left(\frac{8n^2(n+1)\rho^3 + 12n^2\rho^3 + 18n\rho + 9}{\rho^3(2n\rho+3)^2}\right), \tag{5}$$

with $n = \frac{1}{2}(l-1)(l+2)$, where l is the orbital index and for our case $l = 2$. Note that the Zerilli potential decays only algebraically. Due to the nature of the Schwarzschild geometry being static, the variable coefficients of the wave equation are not τ-dependent, so the Laplace transform can be applied to equation (4).

To solve equation (4) numerically, one needs to truncate the numerical domain. Once truncated, the artificial domain boundary may cause non-physical reflections coupled with the potential term if the given boundary condition is not exact. This is because of the long ranging potential term in the equation. If the computational domain is large enough, the boundary effect is reduced. Also, the power-law decay can be obtained inside the computational domain before the boundary effect propagates back to the point where the waveform is collected with time. However, having the computational domain large is computationally expensive. Alternatively, Lau found the exact radiation boundary condition. Lau (2004) developed the non-reflecting boundary condition (NRBC) based on the Laplace transformation technique.

Here we review Lau's method briefly. Applying the formal Laplace transform to equation (4), the following ordinary differential equation (ODE) is obtained:

$$\frac{\partial^2\hat{\Psi}}{\partial\rho_*^2} - (\sigma^2 + V^Z(\rho))\hat{\Psi} = 0. \tag{6}$$

The value of σ is the frequency variable obtained by applying the Laplace transform to the second partial derivative with respect to τ. The variable $\hat{\Psi}$ represents the Laplace transform of the gravitational wave Ψ. The ODE is a special case of the confluent Heun equation which can be solved with a change of variables as outlined in Lau (2004). Since singular points arise in the analysis of the new ODE, the wave equation must be normalised at infinity using transformations. After multiple substitutions in equation (6), the outgoing solution to the ODE in terms of $\hat{\Psi}$, where $\hat{\Psi} = \rho\hat{\psi}$ is one of the substitution variables, is

$$\hat{\psi}(\sigma,\rho) \approx \rho^{-1}e^{\sigma\rho}W_l(\sigma\rho), \tag{7}$$

with $W_l(\sigma\rho) \approx \sum_{n=1}^{\infty}(\sigma\rho)^{-n}$ being the approximate solution to the normalised form of the new ODE. The subscript l is the orbital index. Differentiating equation (7) with respect to ρ and applying the inverse Laplace transform, the equation becomes

$$\frac{1}{U}\frac{\partial\Psi}{\partial\tau} + \frac{1}{T}\frac{\partial\Psi}{\partial\rho} + \frac{1}{T}\frac{\Psi}{\rho} = \rho^{-1}U(\rho)\psi_l(\tau,\rho) * \mathcal{L}^{-1}\left(\sigma\rho\frac{W_l^{'}(\sigma\rho;\sigma)}{W_l(\sigma\rho;\sigma)}\right), \tag{8}$$

where the prime of W is the derivative of W with respect to ρ and the $*$ is Laplace convolution arising from the inverse Laplace transform. The functions T and U are both functions of ρ, specifically $F^{-1/2}(\rho)$ and $F^{1/2}(\rho)$, the radial lapse and temporal lapse functions respectively. These lapse functions are derived from the function $F(\rho)$ in (3). The inverse Laplace transform appearing in the right hand side with the $\Psi(\tau,\rho)$ of equation (8) becomes an integral. Evaluating the solution at the boundary $\rho = \rho_B$, using the substitution $\Psi = \rho\psi$, and returning to the tortoise coordinate for the spatial variable, the exact boundary condition has the following form (Lau, 2004)

$$\left(\frac{\partial\Psi}{\partial\tau} + \frac{\partial\Psi}{\partial\rho_*}\right)\Bigg|_{\rho=\rho_B} = \frac{1-\rho_B^{-1}}{\rho_B}\int_0^{\tau}\omega_2(\tau-\tau';\rho_B)\Psi_2(\tau';\rho_B)d\tau'. \tag{9}$$

The indexing on ω and Ψ refers to the orbital index, $l = 2$, as defined earlier. The function ω represents the compressed Zerilli kernel which is obtained from the inverse Laplace transform in equation (8) and Ψ being the history of the gravitational wave. The method for evaluating the compressed Zerilli kernel and implementation of the exact NRBC will be discussed in the following section.

3 Implementation of boundary conditions

The computational domain is defined in ρ_* and truncated as $\rho_* \in [\rho_*^L, \rho_*^R]$. The left and right boundaries ρ_*^L and ρ_*^R are chosen such that $\rho(\rho_*^L) \sim \rho_e$ and $\rho(\rho_*^R) = 15$ where ρ_e is the size of the horizon. At both boundaries, the radiation boundary conditions should be applied.

3.1 Governing equations

We use the direct form of the gravitational radiation equation equation (4) as the second order partial differential equation (PDE). One can also convert the PDE into a system of equations. The Sommerfeld condition $\Psi_\tau + \Psi_{\rho_*} = 0$, which is the first order PDE, is more appropriate when the equation is converted into the first order system of equations as in Lousto and Price (1997).

3.2 Boundary condition at $\rho_* = \rho_*^L$

We use the following outflow boundary condition at the left domain boundary

$$\left(\frac{\partial\Psi}{\partial\tau} - \frac{\partial\Psi}{\partial\rho_*}\right)\Bigg|_{\rho_*=\rho_*^L} = 0. \tag{10}$$

This boundary condition is not exact because of the potential function V although V is small. The boundary condition is approximated by the first order finite difference method such as

$$\Psi(\rho_*^L, \tau + \Delta t) = \Psi(\rho_*^L, \tau) + \frac{\Delta t}{\Delta \rho_*} \left(\Psi(\rho_*^L + \Delta \rho_*, \tau) - \Psi(\rho_*^L, \tau) \right),$$

where Δt and $\Delta \rho_*$ are the temporal and spatial grid spacing.

3.3 Boundary condition at $\rho_* = \rho_*^R$

For the right boundary we use Lau's NRBC. For the implementation of the NRBC in equation (9), we estimate the kernel ω_2 using a power series and the compressed kernel values from Lau (2004) with $d = 10$. The kernel function ω_2 in equation (9) is approximated by a power series and the compressed kernel values. The series used to estimate ω_2 is

$$\omega_2(\tau - \tau') \approx \sum_{k=1}^{d} \gamma_k e^{\beta_k(\tau - \tau')}. \tag{11}$$

The values of β_k and γ_k are adopted from Table II for the compressed Zerilli kernels in Lau (2004). Those values in Table II in Lau (2004) were obtained specifically for those when $\rho_B = 15$.

Using the above approximation, the right hand side of equation (9), i.e., the integral convolution, can be simplified. We take the right hand side of equation (9) to be the following

$$A(\tau + \Delta t) = \frac{F(\rho_B)}{\rho_B} \sum_{k=1}^{d} \int_0^{\tau + \Delta t} \gamma_k e^{\beta_k(\tau + \Delta t - \tau')} \Psi(\tau') d\tau', \tag{12}$$

where $F(\rho_B) = 1 - \rho_B^{-1}$. We define $C_k(\tau + \Delta t)$ to be the integral on the right hand side of equation (12) as below

$$C_k(\tau + \Delta t) = \sum_{k=1}^{d} \gamma_k e^{\beta_k(\tau + \Delta t)} \int_0^{\tau + \Delta t} e^{-\beta_k \tau'} \Psi(\tau') d\tau'. \tag{13}$$

This integral can be broken into two parts; the first integral being evaluated from 0 to τ and the second being evaluated from τ to $\tau + \Delta t$. By definition we have

$$C_k(\tau + \Delta t) = e^{\beta_k \Delta t}(C_k(\tau) + B_k(\tau)), \tag{14}$$

where $C_k(\tau)$ and $B_k(\tau)$ are

$$C_k(\tau) = \gamma_k e^{\beta_k \tau} \int_0^{\tau} e^{-\beta_k \tau'} \Psi(\tau') d\tau', \tag{15}$$

$$B_k(\tau) = \gamma_k e^{\beta_k \tau} \int_{\tau}^{\tau + \Delta t} e^{-\beta_k \tau'} \Psi(\tau') d\tau'. \tag{16}$$

With the definition of $C_k(\tau+\Delta t)$, $A(\tau+\Delta t)$ rewritten as

$$A(\tau+\Delta t)=\frac{F(\rho_B)}{\rho_B}\left[\sum_{k=1}^{d}e^{\beta_k\Delta t}C_k(\tau)+\sum_{k=1}^{d}e^{\beta_k\Delta t}B_k(\tau)\right]. \tag{17}$$

For the integral of $B_k(\tau)$, we use the first order approximation of Ψ such that

$$\Psi(\tau')=\frac{\Psi(\tau+\Delta t)-\Psi(\tau)}{\Delta t}(\tau'-\tau)+\Psi(\tau), \tag{18}$$

where $\Psi(\tau+\Delta t)$ is unknown at the current time, $\tau'=\tau+\Delta t$, and $\Psi(\tau)$ is known from the previous time, $\tau'=\tau$. Making this substitution into the equation for $B_k(\tau)$, the new form of $B_k(\tau)$ becomes

$$B_k(\tau)=\gamma_k\left(\left[\frac{\Psi(\tau+\Delta t)-\Psi(\tau)}{\Delta t}\right]D_k+\Psi(\tau)E_k\right), \tag{19}$$

where D_k and E_k are coefficients defined as

$$D_k=\frac{1}{\beta_k^2}\left(1-e^{-\beta_k\Delta t}[1+\beta_k]\right), \tag{20}$$

$$E_k=\frac{1}{\beta_k}[1-e^{-\beta_k\Delta t}]. \tag{21}$$

To find the boundary value of $\Psi(\rho_*^R)$, we use the explicit forward difference method using the exact NRBC which is given by

$$\frac{\Psi(\rho_*^R,\tau+\Delta t)-\Psi(\rho_*^R,\tau)}{\Delta t}=-\frac{\Psi(\rho_*^R,\tau)-\Psi(\rho_*^R-\Delta\rho_*,\tau)}{\Delta\rho_*}+A(\tau+\Delta t), \tag{22}$$

where $\Psi(\rho_*^R,\tau+\Delta t)$ is the unknown value of Ψ, $\Psi(\rho_*^R,\tau)$ and $\Psi(\rho_*^R-\Delta\rho_*,\tau)$ are the previous values of Ψ, and $\Delta\rho_*$ is the grid spacing at the domain boundary. With $A(\tau+\Delta t)$, $\Psi(\rho_*^R,\tau+\Delta t)$ is then given by

$$\Psi(\rho_*^R,\tau+\Delta t)=\frac{\Psi(\rho_*^R,\tau)-H(\Psi^n)+\Delta t\frac{F(\rho_*^R)}{\rho_*^R}[J_k(\tau)]\Psi(\rho_*^R,\tau)}{1-\frac{F(\rho_B)}{\rho_B}\sum_{k=1}^{d}e^{\beta_k\Delta t}\gamma_kD_k}, \tag{23}$$

where $H(\Psi^n)$ and $J_k(\tau)$ are defined as

$$H=\frac{\Delta t}{\Delta\rho_*}[\Psi(\rho_*^R,\tau)-\Psi(\rho_*^R-\Delta\rho_*,\tau)], \tag{24}$$

$$J_k=\left[\sum_{k=1}^{d}e^{\beta_k\Delta t}(C_k(\tau)+\gamma_k\left(E_k-\frac{1}{\Delta t}D_k\right))\right]. \tag{25}$$

4 Multi-domain spectral and finite difference methods

To solve equation (4), we use our previous hybrid method (Chakraborty et al., 2011) based on the multi-domain spectral and finite difference methods for the spatial derivatives. For the temporal derivative, we use the second order finite difference method based on the two step methods. In our previous work, we showed that the hybrid method is better performing than the finite difference or spectral methods and reduces the computational cost significantly. The main motivation of using the hyrbid method in this work is to examine wether we can further enhance the computational efficiency with the exact NRBC.

The computational domain is partitioned into the multi-domain spectral domains and the finite difference domain. The finite difference domain serves as the boundary domain. Each spectral domain uses the Chebyshev spectral method and the size of all the spectral domains is same. Equation (4) is solved in each subdomain and the solution is patched across the domain interface. The spectral filtering method is also applied in each spectral domain if necessary.

4.1 Patching for spectral domains

Consider the two adjacent spectral (SP) domains Ω_s^i and Ω_s^{i+1} whose solutions are denoted by ϕ and ψ, respectively. The superscripts i and $i+1$ denote the i^{th} and $(i+1)^{\text{th}}$ domains, respectively. The subscript s denotes that the domain is the spectral domain. Hereafter, let ϕ and ψ denote the solution in the left and the right sub-domains, respectively. Using the three consecutive grids up to the domain interface point, we use the fourth order approximation to patch the solution at the domain interface as follows

$$\phi_0^{j+1} = 2\phi_0^j - \phi_0^{j-1} + \Delta t^2 \frac{-\psi^j_{N^i-2} + \lambda^4 \psi^j_{N^i-1} - 2(\lambda^4-1)\phi_0^j + \lambda^4\phi_1^j - \phi_2^j}{h_o^2\lambda^2(\lambda^2-1)}, \tag{26}$$

where the superscripts $j+1$, j, and $j-1$ indicate the time steps $(j+1)\Delta t$, $j\Delta t$, and $(j-1)\Delta t$ and $h_o = x_1^{i+1} - x_0^{i+1}$ and $\lambda = (x_2^{i+1} - x_0^{i+1})/h_o$. N^i denotes the polynomial order in the i^{th} subdomain. In this work, we choose $N^i = N$ for all i for the spectral subdomains. The value x_k denotes the k^{th} collocation point in each domain. Each spectral domain has the same domain size. Thus $x_2^{i+1} - x_0^{i+1} = x^i_{N^i} - x^i_{N^i-2}$ with $h_o = x^i_{N^i} - x^i_{N^i-1}$.

Figure 1 (Chakraborty et al., 2011) shows the schematic illustration of the adjacent spectral subdomain interface and patching scheme. The spectral ghost cells are the grid points in the neighbouring subdomain that are needed for the fourth order interpolation. Since every subdomain has the same domain size and the polynomial order is same in every spectral domain, the spectral ghost cells coincide with the collocation points in the neighbouring subdomain.

For the left domain Ω_s^i, the right boundary value is updated in the same way:

$$\begin{aligned}\psi_{N^i}^{j+1} = {} & 2\psi_{N^i}^j - \psi_{N^i}^{j-1} \\ & + \Delta t^2 \frac{-\psi^j_{N^i-2} + \lambda^4 \psi^j_{N^i-1} - 2(\lambda^4-1)\psi^j_{N^i} + \lambda^4\phi_1^j - \phi_2^j}{h_o^2\lambda^2(\lambda^2-1)}.\end{aligned} \tag{27}$$

Once ψ and ϕ are updated at the domain interface, we use the averaging method to update the final value of the solution at the interface.

Figure 1 SP-SP patching at the interface (pointed by arrow)

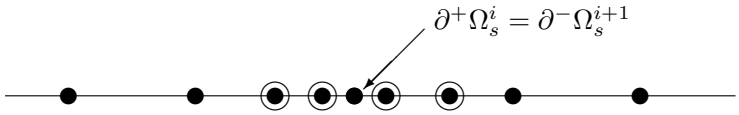

Notes: • Spectral grids, ◯ Spectral ghost cells

4.2 Patching for the spectral and finite difference domains

For the spectral and finite difference (FD) domain patching, we use the polynomial interpolation for the ghost cells because the ghost cells do not coincide with the collocation points in the neighbouring subdomain. Here note that we use the uniform spacing for the finite difference domain. We use the same fourth order interpolation. Let ψ and ϕ be the solutions in the finite difference domain Ω_f^i and spectral domain Ω_s^{i-1}, respectively, where the subscript f denotes the domain by the finite difference method. Figure 2 (Chakraborty et al., 2011) shows the ghost cells in this case and the patching method.

Figure 2 SP-FD patching at the interface (pointed by arrow)

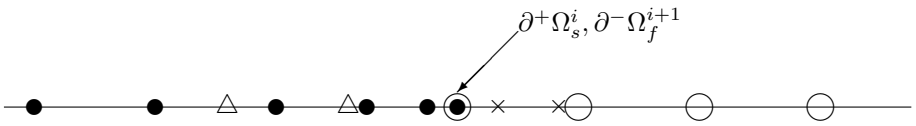

Notes: ◯ Finite-difference grid points, △ Finite-difference ghost cells
• Spectral grid points, × Spectral ghost cells

The value of ψ at the left boundary of Ω_f^i is updated using the following:

$$\psi_0^{j+1} = 2\psi_0^j - \psi_0^{j-1} + (\Delta t)^2 \frac{-\psi_2^j + 16\psi_1^j - 30\psi_0^j + 16\Psi_1^j - \Psi_2^j}{12h_f^2}, \tag{28}$$

where $h_f = x_1^i - x_0^i$ and

$$\Psi_l^j = \sum_{k=0}^{N^{i-1}} U(x_k^{i-1}) L_k \left[\xi(x_{N^{i-1}}^{i-1} + lh_f)\right], \quad l = 1, 2.$$

Here $L_k(w)$ is the Lagrange interpolation polynomial based on the Chebyshev polynomials given by

$$L_k(w) = \frac{(-1)^{N^{i-1}}(1-w^2)T'_{N^{i-1}}(w)}{\bar{c}_k {N^{i-1}}^2 (w - w_k)},$$

where $\bar{c}_j = 2$ if $j = 0, N^{i-1}$ and $\bar{c}_j = 1$ otherwise (Hesthaven et al., 2009) and $T'_{N^{i-1}}(w)$ is the first derivative of the Chebyshev polynomial of degree N^{i-1} with respect to w. The value of ϕ at the left boundary Ω_s^{i-1} is updated in the similar way, but using the non-uniform formula equation (26), we have

$$\phi_{N^{i-1}}^{j+1} = 2\phi_{N^{i-1}}^{j} - \phi_{N^{i-1}}^{j-1} + (\Delta t)^2 \frac{-\Phi_1^j + \lambda^4 \Phi_0^j - 2(\lambda^4 - 1)\phi_{N^{i-1}}^j + \lambda^4 \phi_{N^{i-1}-1}^j - \phi_{N^{i-1}-2}^j}{h_0^2 \lambda^2 (\lambda^2 - 1)}, \quad (29)$$

where h_0 and λ are defined in the same way as in equation (26). The interpolation Φ_l^j are determined by

$$\Phi_m^j = \sum_{k=0}^{4} U^i(z_k) \prod_{l=0, l\neq k}^{4} \frac{y_m - z_l}{z_k - z_l}, \quad m = 0, 1,$$

where $z_k = x_k^i$ and

$$y_m = x_0^i + h_0 \lambda^m, \quad m = 0, 1.$$

Once the solution is updated at the domain interface, we also use the average value of ϕ and ψ to update the final solution value at the domain interface.

4.3 Filtering methods

To reduce the oscillatory behaviour caused by the non-physical reflections at ρ_*^L and ρ_*^R, we apply the filtering method for the spectral domain. For the spectral domain we apply the exponential filter. The exponential filter of order q is used

$$\sigma(\theta) = e^{-\alpha|\theta|^q}, \quad \alpha > 0, \quad (30)$$

where (30) is a real, even function. The filtered Chebyshev approximation is given by Hesthaven et al. (2009)

$$F_N(x) = \sum_{n=0}^{N} \sigma\left(\frac{n}{N}\right) a_n T_n(x).$$

5 Numerical results

We solve equation (4) using the second order two step method for the temporal derivative and the hybrid method for the spatial derivatives. We use a smooth Gaussian profile for the initial condition defined below

$$\Psi(\rho_*, \tau = 0) = \exp(-\frac{1}{10}(\rho_* - \rho_*^o)^2),$$

where $\rho_*^o = -50$. The polynomial order, p_s, and the total number of subdomains, N_t, are chosen such that the Gaussian profile is smooth enough within each subdomain.

In this work, we choose $p_s = 16$ and various values of N_t including $N_t = 1,000$. The number of grid points in the finite difference domain is automatically determined once the grid resolution in the spectral domain is determined such that the grid homogeneity is maintained across the domain interface between the spectral and finite difference domains. The initial Gaussian profile satisfies the following condition at $\tau = 0$

$$\frac{\partial \Psi}{\partial \tau} + \frac{\partial \Psi}{\partial \rho_*} = 0. \tag{31}$$

The interface of the spectral and finite difference domains is at $\rho = 12$. The outer boundary of the finite difference domain is at $\rho = \rho_B = 15$.

In this work we consider the following three cases:

- Case I: Equation (31) is used as the boundary condition at $\rho = \rho_B$ for all $\tau > 0$
- Case II: Lau's analytic boundary condition is used at $\rho = \rho_B$
- Case III: The spectral filtering method is applied within the spectral domain for Case II.

5.1 Case I

Figure 3 shows the late-time waveform of $|\Psi|$ versus τ collected at $\rho = 3.64784$ (red) and the domain boundary $\rho_B = 15$ (blue). Here note that $\rho = 3.64784$ is located inside the spectral domain. As shown in the figure, the waveform at $\rho_* = \rho_*^R$ is decaying with τ up to 10^{-11} until it grows again from $\tau \sim 10^{2.45}$. The waveform at $\rho = 3.64784$ shows the similar decay pattern but a plateau of $\sim 10^{-10}$ lasts until the boundary effect affects it. As we see in Figure 6, the level of the plateau is corresponding to the magnitude of $|\Psi|$ at $\rho = 15$ when computed with the first order outflow boundary condition with $V = 0$. For this case, no power-law decay behaviour is obtained even for an extended time interval.

Figure 3 Case I: Late-time decay of $|\Psi|$ at $\rho_B = 15$ (blue) and at $\rho = 3.64784$ (red) with the first order outflow boundary condition (see online version for colours)

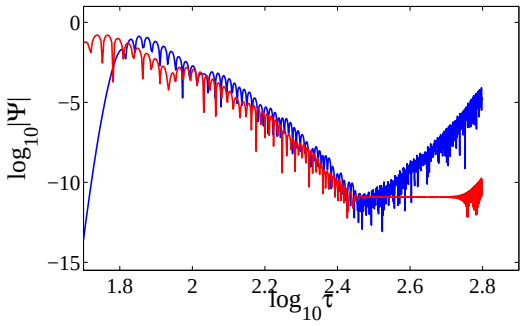

Figure 4 Case II: Late-time decay of $|\Psi|$ at $\rho_B = 15$ (blue) and at $\rho = 3.64784$ (red) with Lau's NRBC (see online version for colours)

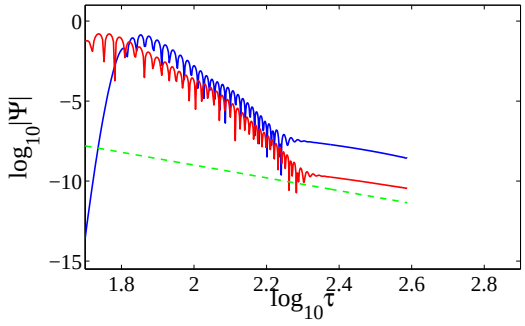

Note: The green dashed line is the reference line with $p = -4$.

5.2 Case II

In Case II, we solve equation (4) with Lau's boundary condition. Figure 4 shows that the quasi-normal ringing is observed along with the power-law decay at both locations of $\rho = 15$ and $\rho = 3.64784$. The t^p fall-off is plotted with the power $p = -4.0$ as a reference line in green. Using Lau's exact boundary condition at $\rho = \rho_B = 15$, a power-law decay is obtained, but not of the correct order. The true value of the power-law decay in the Zerilli case for $l = 2$, should be $p = -7$. This result implies that Lau's exact boundary condition is indeed superior to the homogeneous Sommerfeld condition, but is not enough with the given values of p_s and N_t. When the potential term V vanishes, the homogeneous Sommerfeld condition is exact for the second order wave equations. However, computationally it is not exact. That is, there exists the non-vanishing reflection mode due to the finite discretisation of space and time although it is small. Figure 6 shows such an inexactness. To reduce this problem, the discretisation of space and time seems to be required small enough. But it turns out, in the following, that increasing the grid resolution does not improve the result. Similar phenomenon is reported in Khanna (2013). This is because of the errors by such a computational inexactness. Rewriting the given wave equation into a system or using the higher precision and high-order method would be a better approach to reduce the inexactness as suggested in Khanna (2013).

5.3 Case III

Case III uses the spectral filtering method with the identical exact boundary condition as in Case II. The filtering orders used are $q = 16, 12, 10, 8$. Figure 5 shows the late-time profile of the waveform both at $\rho = 15$ (Blue) and at $\rho = 3.64784$ (Red). The figure shows that the power-law decay profile is obtained with the similar order of $p \sim -4$. For $q = 8$ (bottom right), the decay profile is oscillatory at $\rho = 3.64784$ but the overall power-law decay is still $p \sim -4$. As shown in the figure the filtering method does not help to improve the result in terms of the order of the power-law decay.

Figure 5 Case III: Late-time decay of Ψ at $\rho = 15$ (Blue) and at $\rho = 3.64784$ (Red) with Lau's NRBC and spectral filtering method (see online version for colours)

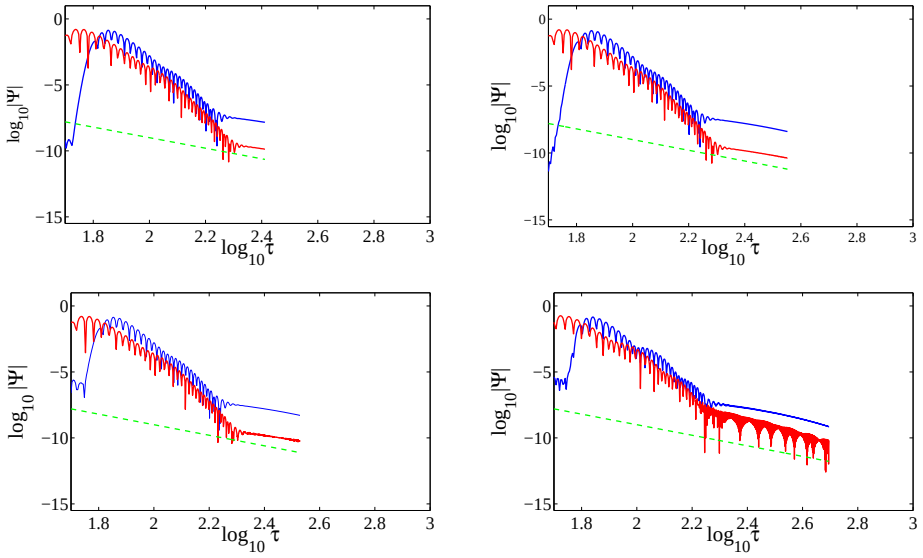

Note: $q = 16, 12, 10, 8$ from top to bottom and left to right.

We explain the reasons why the proper power-law decay is not obtained with Lau's method are as follows. First of all, the computational implementation of the first order outflow boundary condition is not *exact* even for $V = 0$ in the sense that there exists the reflecting mode at the domain boundary although it is small. As Figure 6 shows the reflecting mode is significant at the domain boundary unless the temporal and spatial steps are small enough that the reflecting mode is negligible. Second, the coupling of the produced non-physical reflections with the potential term hinders us from obtaining the proper power-law decay. To remedy this problem, the value of ρ_B must be increased or the temporal and spatial resolution should be decreased significantly.

To see such numerical effect, we solve equation (4) with the vanishing potential function V. When $V = 0$, equation (4) is a simple wave equation in $1 + 1$ space-time and the Sommerfeld condition at $\rho = \rho_B$ is theorectically exact. Figure 6 shows the late-time decay behaviour of Ψ for the vanishing potential with the outflow boundary condition $\Psi_\tau + \Psi_{\rho_*} = 0$ collected at $\rho = \rho_B$ (top figure) and the profile of $|\Psi|$ versus ρ_* at $\tau = 10^{2.3345}$ (bottom figure). To avoid possible non-physical reflections from the left boundary at $\rho_* = \rho_*^L$, we use $\rho_*^L = -1,000$. As shown in the figure, the Gaussian profile exits the domain and Ψ decays as it propagates toward the boundary. However, the outflow boundary condition is exact only up to 10^{-10} at $\rho = 15$ for $p_s = 16$ and $N_t = 1,000$ and the reflected wave propagates to left from the right boundary (bottom figure). The magnitude of the reflected wave is significantly large, $\sim 10^{-4}$, compared to the magnitude of Ψ, $|\Psi| \sim 10^{-10}$, at $\rho = \rho_B$, which results in disturbing the waveform collected inside the domain when coupled with the potential term.

Figure 6 Ψ with $V = 0$. The first order PDE, $\Psi_\tau + \Psi_{\rho_*} = 0$, is used as the boundary condition (see online version for colours)

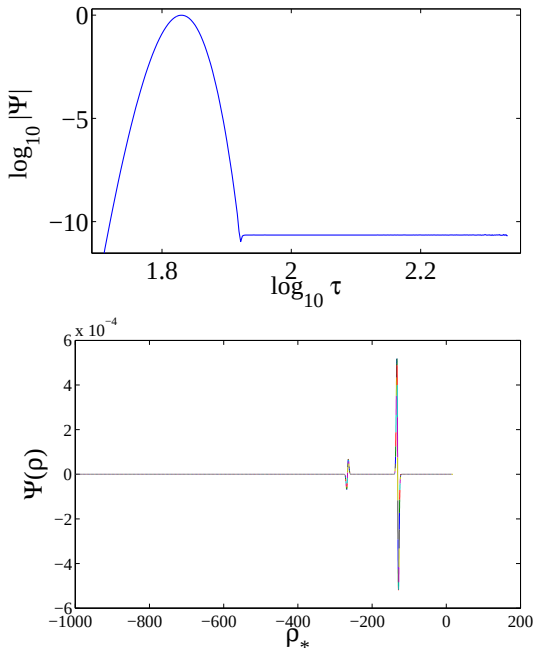

Notes: Top: Late-time decay of Ψ at $\rho = \rho_B$. Bottom: Ψ versus ρ_* at $\tau = 10^{2.3345}$.

In order to reduce the errors due to the inexactness in Figure 6, we examine various grid resolutions and the size of the domain boundary. Figures 7 and 8 show more results with Lau's NRBC. The solid line in purple color is the reference line with the power $p = -4$. Figure 7 shows the power-law decay with different $\rho_B \geq 15$, $\rho_B = 15, 16, 18, 19$ (from left to right, top to bottom). Figure 8 shows the power-law decay with higher grid resolutions $N_t = 1,000, 1,200, 1,500, 1,800$ (from left to right, top to bottom). The grid resolution in the finite difference domain changes according to the requirement of the grid homogeneity between the spectral and finite difference domains. As shown in these figures, the similar power-law decay patterns are observed for every case. As these figures indicate, the grid resolution does not improve the result when the domain boundary is still small $\rho_B \sim 19$. The inexactness errors are still significant as long as the first order radiation boundary condition is incorporated in the second order wave equation if the domain boundary is small enough.

Figure 7 Late-time decay of $|\Psi|$ with $\rho_B = 15, 16, 18, 19$ (from left to right and top to bottom) (see online version for colours)

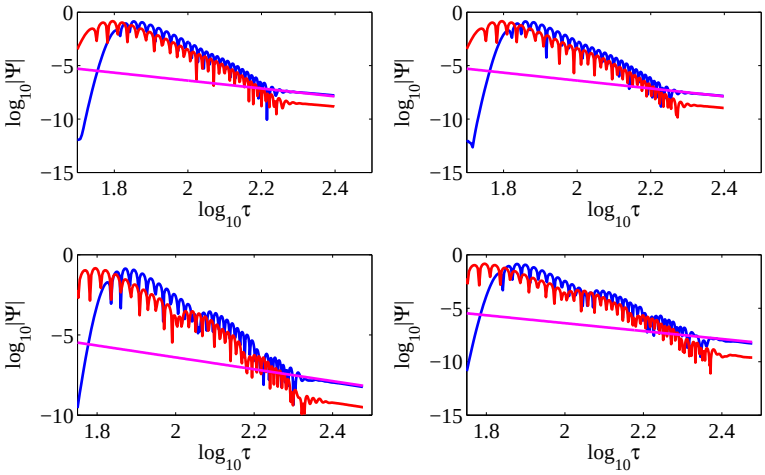

Figure 8 Late-time decay of Ψ with different resolutions, $N_t = 1,000, 1,200, 1,500, 1,800$ (from left to right and top to bottom) (see online version for colours)

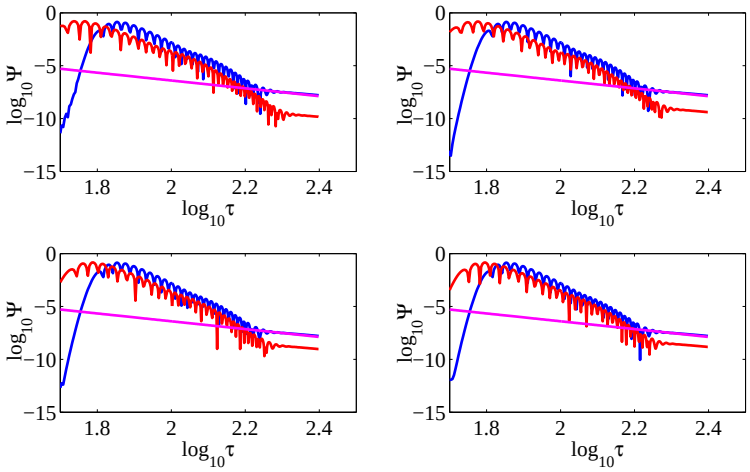

6 Conclusions

In this note, we solve the Zerilli equation on the Schwarzschild background. The second order wave equation is solved using the spectral and finite difference hybrid method. The computational domain is split into the finite difference domain and the spectral domain. The spectral domain is split into multiple subdomains, each of which solves the wave equation with the Chebyshev spectral method. For the right boundary, we use Lau's analytic boundary condition developed by Lau (2004) based on the Laplace transformation. In this note, we present several numerical experiments with Lau's method. Our numerical results show that the power-law decay at a slower rate is

obtained with Lau's exact boundary condition with the small value of the right boundary location. But the expected power-law of the order $p = -7$ is not obtained. The obtained order is about $p \sim -4$. Our numerical results show that the filtering method does not help to improve the result. The exact boundary condition is given by the first order wave equation with the source term. Due to the finite resolution with the finite precision, there exists a non-physical reflecting mode at the domain boundary. The inexactness errors still significant as long as the first order radiation boundary condition is incorporated in the second order wave equation when the domain boundary is small. Thus the main observation in this paper is that our hybrid method yields the proper power-law decay even with the first order homogeneous Sommerfeld boundary condition with a relatively small value of ρ_B, but if ρ_B is extremely small, e.g., $\rho_B \sim 19$, the inexactness error becomes dominant with the coupling of the non-zero potential term and higher resolution does not improve the performance. In Khanna (2013), it is shown that in such a case high order implementation or high precision computation can remedy the problem. Thus we propose to use the hybrid method with more consistent formulation, such as the system of the first order wave equation with the first order NRBC or to use a high precision computation. Both approaches will enhance the computational efficiency by hybridising the spectral and finite difference methods.

Acknowledgements

The authors thank Stephen Lau for his kind and detailed communication and his valuable teaching on the analytic boundary condition and thank Scott Field for his useful comments on Lau's analytic boundary condition. The authors also thank the organisers of the 3rd New York Conference on Applied Mathematics (NYCAM), which was held in October in 2012 at RPI. This paper is submitted for the NYCAM conference special issue.

References

Avalos, E. and Lousto, C. (2005) 'Numerical integration of the Teukolsky equation in the time domain, *Phys. Rev. D*, Vol. 72, No. 8, pp.84022–84039.

Baumgarte, T.W. and Shapiro, S.L. (2011) 'Binary black hole merger', *Physics Today*, pp.32–37.

Benedict, A.G., Field, S.E. and Lau, S.R. (2012) 'Fast evaulation of asymptotic waveforms from gravitational perturbations', arXiv:1210.1565.

Chakraborty, D., Jung, J-H. and Khanna, G. (2011) 'A multi-domain hybrid method for head-on collision of black-holes in particle limit', *Intl. J. of Mod. Phys. C*, Vol. 22, No. 5, pp.517–541.

Davis, M., Ruffini, R., Press, W.H. and Price, R.H. (1971) 'Gravitational radiation from a particle falling radially into a Schwarzschild black hole', *Phys. Rev. Lett.*, Vol. 27, pp.1466–1469.

Glampedakis, K. (2005) 'Extreme mass ratio inspirals: LISA's unique probe of black hole gravity', *Class. Quant. Grav.*, Vol. 22, No. 15, pp.S605–S659.

Hesthaven, J., Gottlieb, D. and Gottlieb, S. (2009) *Spectral Methods for Time-dependent Problems*, Cambridge UP, Cambridge.

Jung, J-H., Khanna, G. and Nagle, I. (2009) 'A spectral collocation approximation of one-dimensional head-on collisions of black holes', *Intl. J. of Mod. Phys. C*, Vol. 20, No. 11, pp.1827–1848.

Khanna, G. (2013) 'High-precision numerical simulations on a CUDA GPU: Kerr black hole tails', *J. Sci. Comput.*, Vol. 56, No. 2, pp.366–380.

Lau, S.R. (2004) 'Rapid evaluation of radiation boundary kernels for time-domain wave propagation on blackholes', *J. Comp. Phys.*, Vol. 199, No. 1, pp.376–422.

Lousto, C. and Price, R. (1997) 'Head-on collisions of black holes: the particle limit', *Phys. Rev. D*, Vol. 55, No. 4, pp.2124–2138.

Price, R.H. (1972) 'Nonspherical perturbations of relativistic gravitational collapse. 1. Scalar and gravitational perturbation', *Phys. Rev. D*, Vol. 5, No. 10, pp.2419–2439.

Price, R.H. and Pullin, J. (1994) 'Colloiding black holes: the close limit', *Phys. Rev. Lett.*, Vol. 72, No. 21, pp.3297–3300.

Zerilli, F.J. (1970) 'Gravitational field of a particle falling in a Schwarzschild geometry analyzed in tensor harmonics', *Phys. Rev. D*, Vol. 2, No. 10, pp.2141–2160.